Turkish Journal of Electrical Engineering & Computer Sciences

http://journals.tubitak.gov.tr/elektrik/

Research Article

Turk J Elec Eng & Comp Sci
(2015) 23: 945 – 955

doi:10.3906/elk-1304-145

Design and analysis of EI core structured transverse flux linear reluctance actuator

Ahmet FENERCİOĞLU[1,*], **Yusuf AVŞAR**[2]

[1]Department of Mechatronics Engineering, Faculty of Engineering and Natural Science, Gaziosmanpaşa University, Tokat, Turkey

[2]Department of Electronics and Automation, İpsala Vocational College, Trakya University, İpsala, Edirne, Turkey

Received: 16.04.2013 • **Accepted/Published Online:** 26.06.2013 • **Printed:** 10.06.2015

Abstract: In this study, an EI core linear actuator is proposed for horizontal movement systems. It is a transverse flux linear switched reluctance motor designed with an EI core structure geometrically. The actuator is configured into three phases and at a 6/4 pole ratio, and it has a stationary active stator along with a sliding passive translator. The stator consists of E cores and the translator consists of I cores. The actuator has a yokeless design because the stator and translator have no back iron. The E and I cores are separated from each other to provide a fault-tolerant design and decrease the weight. The proposed model is analyzed by 3D finite element method. Phase inductance, flux linkage, and axial forces are examined by magnetostatic finite element analysis and verified by analytical approximations and experimental results. Under DC 8 A phase excitation, propulsion force is 72.57 N and corresponding power consumption is 115.5 W. This has advantages for horizontal movement systems.

Key words: Transverse flux switched reluctance motor, linear switched reluctance motor, linear actuator

1. Introduction

Conventional linear systems are driven by a rotational motor, which is mechanized with a pulley or chain drive system. These types of mechanisms can cause faults and require periodical maintenance. Mechanical transmissions that are converted from rotational movement to linear movement cause power losses. In addition, rotational electrical motors create vibrations. The proposed linear actuator implements electromechanical energy conversion as a direct drive. Mechanical transmissions are not necessary because linear movement forces are transferred magnetically. The actuator has a simple geometrical structure and it does not require a permanent magnet; therefore, its design and manufacturing costs are low [1]. It is a design that is fault-tolerant and energy-efficient. It requires a driver circuit and position information for the control system. The driver is easier to apply than the commonly used induction motor's drivers. The developing power electronics components and microcontrollers enable usage in linear moving systems with an easy and flexible control strategy. Iancu et al. [2] presented modular structured transverse flux switched reluctance machines. The fault characteristics of linear and tubular transverse flux reluctance machines were examined in their modular construction. The aspects related to the functioning in fault conditions are presented. Baoming et al. [3] presented design procedures of a transverse flux linear switched reluctance motor (LSRM) that had 12 primary poles, 3 phases, and 250 W power. The analytical design was verified by finite element analysis (FEA) and experimental results.

*Correspondence: ahmet.fenercioglu@gop.edu.tr

Calculated and experimental results validated the design procedure with 5% tolerance. Another study [4] dealt with the design of a new LSRM. The LSRM was proposed as triple-sided to generate high force and to provide a MagLev effect so that friction force was reduced. The LSRM was analyzed by FEA and verified by analytical methods. The new motor had advantages such as low cost and simple structure. It was proposed for railway transportation systems. In [5], a transverse flux reluctance motor was modeled as a circuit-field based on a variable equivalent air gap permeance concept. The BH curve of the core along with the saturation factor was considered. Simplified model parameters and the calculated values were compared and verified by finite element method (FEM) analysis. The model provided simple analytical expressions useful for dynamic analysis. In the literature [6], a circular flux linear actuator was designed as double-sided with a circular structure. Its 3D FEA and analytical approach were examined. It had an active translator and passive stator. The circular structure provided uniform flux distribution and reduced the saturation effects and leakage flux. In [7], a longitudinal flux double-sided LSRM was designed, analyzed, and proposed for a prototype elevator. Its fuzzy logic control of the velocity was simulated [7,8]. Lenin and Arumugam [9] carried out a detailed sensitivity analysis of the effect of geometrical parameters on the performance of a single-sided longitudinal flux LSRM and proposed linear propulsion drives. LSRM drives were investigated and proven to be an alternative actuator for vertical linear elevators [10]. This study includes the design and FEA of a transverse flux one-sided LSRM with EI core structure. Magnetic parameters of the proposed actuator such as phase inductance, flux linkage, flux density in air gap, and forces are examined by FEA and analytical approximations.

2. EI core linear actuator

The iron sheets are stamped out in E and I shapes and are stacked as an EI core with a 3-legged structure. Coils can be wound around any leg, but usually the center leg is used. This is a shell type core and is used more for power transformers, autotransformers, and inductors. In rapidly changing field applications such as in a transformer, the EI iron sheets are laminated as thin (0.25–0.50 mm) and insulated to prevent eddy current losses. EI cores have higher flux path cross-sections than UI cores, so he wide magnetic coupling area generates high force. It is obtained from transformer manufacturers easily and cheaply. The simulator and real prototype models of the actuator are shown in Figure 1.

The LSRM is divided into two pairs of their magnetic flux directions, these being transverse or longitudinal flux structurally. Either can be designed as single- or double-sided [11]. The actuator consists of a stator and translator parts. The stator is the fixed part and is called a passive stator because it has no coils on it. The translator is the moving part and is called an active translator because it has coils. The three-phase linear actuator has a 6/4 pole ratio and each phase has two excited coils. The phase excitation sequence depends on the translator position and movement direction. The translator moves 30 mm when a phase excitation is completed, so it moves 90 mm when 3 phases are excited, respectively. Phase switching and movement start in an overlapping position. In the fully aligned position, the excitation is turned off because this position is the brake region for the aligned phase. In this case, the other overlapping phase is switched on, so it requires position information. According to this information, which is obtained from the sensor, the driver circuit controls the linear actuator [12]. Sizes of the proposed linear actuator are presented in Figure 2 and Table 1.

3. Assumptions

The simulator model of the proposed linear actuator is magnetostatically analyzed by 3-dimensional FEA. Effects of saturation, fringing, leakage flux, end windings effects [13], and skewing are included in the solution

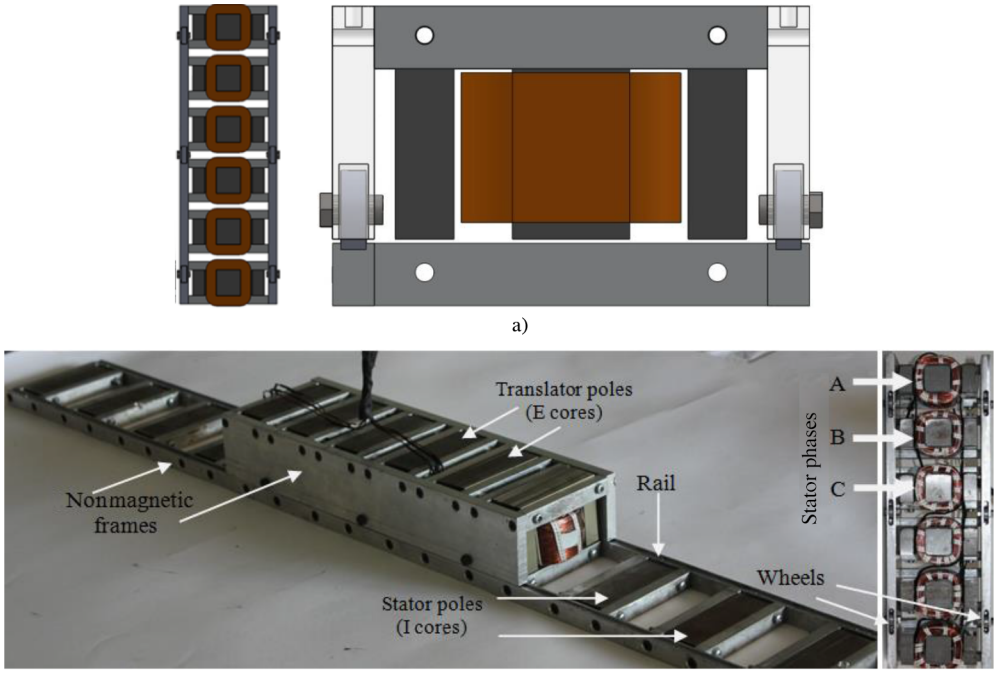

Figure 1. Simulator and real prototype models of the linear actuator: (a) front-rear view, (b) real prototype model.

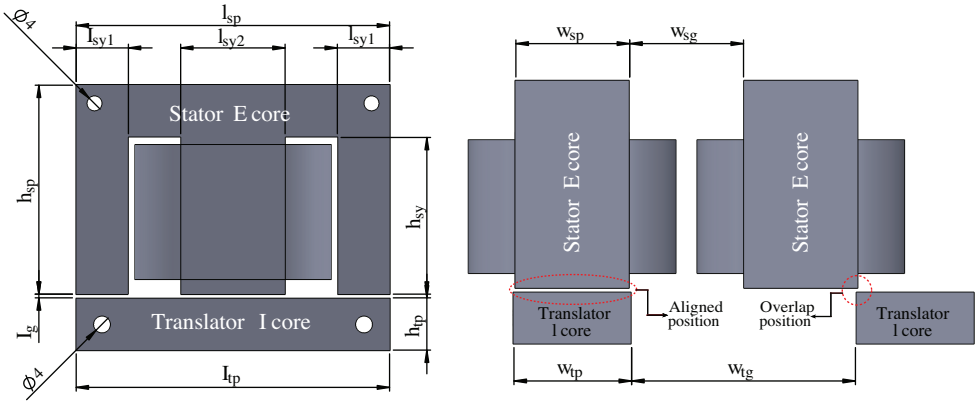

Figure 2. Sizes of proposed linear actuator.

Table 1. Geometrical sizes of the actuator.

Symbol	Dimensions	Size (m)	Symbol	Dimensions	Size (m)
l_{sp}	Length of stator pole	0.084	w_{sp}	Width of stator pole	0.030
l_{sy1}	Length of stator yoke 1	0.014	w_{sg}	Gap of stator poles	0.030
l_{sy2}	Length of stator yoke 2	0.028	w_{tp}	Width of translator pole	0.031
l_{tp}	Length of translator pole	0.084	w_{tg}	Gap of translator poles	0.059
h_{sp}	Height of stator pole	0.056	l_s	Length of overall stator	0.33
h_{sy}	Height of stator yoke	0.042	n_{sp}	Number of stator poles	6
h_{tp}	Height of translator pole	0.014	n_{tp}	Number of translator poles	12
l_g	Length of air gap	0.001	m	Number of phase	3

[14]. Results of the analysis are thus reliable. Dirichlet boundary conditions are twice greater than the model in three axes because it has uniform conditions [1]. In FEA analysis, BH characteristics of the core material are taken into consideration and the BH curve is given in Figure 3. Each phase consists of two serially connected copper coils, which are single solid parts. The phase is excited by magnetomotive force (mmf) at ampere-turn 500 At, 1000 At, 1500 At, 2000 At, 2500 At, and 3000 At respectively in analysis. Consequently, phase excitations are assumed to be 2 A, 4 A, 6 A, 8 A, 10 A, and 12 A because the turn number of a coil is considered as 250. Magnetostatic FEA analysis and analytical solutions are made for each millimeter of translator positions. Lamination, dynamic model, driver and switching effects, and control strategies are not taken into consideration. In analytical approximations, it is assumed that the BH curve is linear in calculation of L_a, L_u, and L_m inductances, so ψ_r is constant and flux distribution is uniform.

4. Electromagnetic model of the actuator

4.1. Magnetic circuit

The EI core is combined with two UI cores, so it has a joint flux in the center leg and twin flux paths in the other legs of the E core. The ϕ_1, ϕ_2 fluxes are joined at the center of the E core. Therefore, its pole length (l_{sy2}) must be twice greater than (l_{sy1}) in order not to saturate the E core [7,15]. The magnetic circuit of the EI cores is shown in Figure 4 and parameters are given in Table 2. To derive phase inductance of the actuator, reluctances are calculated respectively via Eqs. (1)–(6).

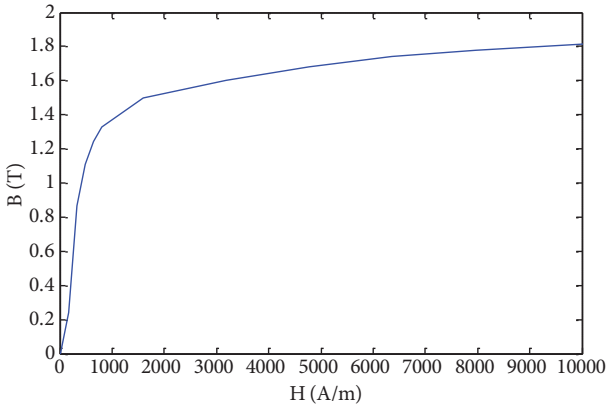

Figure 3. BH curve of the core material.

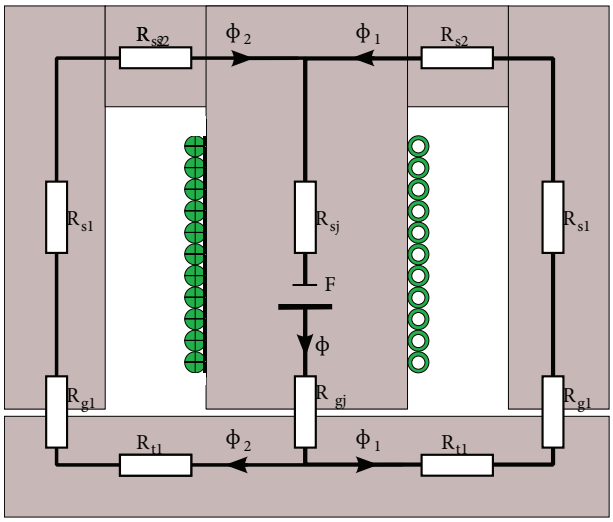

Figure 4. Magnetic circuit of EI core.

$$R_{s1} = \frac{h_{sp}}{\mu l_{sy1} w_{sp}} \tag{1}$$

$$R_{s2} = \frac{l_{sp} - (l_{sy2} + 2l_{sy1})}{2\mu(h_{sp} - h_{sy}) w_{sp}} \tag{2}$$

$$R_{sj} = \frac{h_{sp}}{\mu l_{sy2} w_{sp}} \tag{3}$$

$$R_{t1} = \frac{l_{tp}}{2\mu h_{tp} w_{tp}} \tag{4}$$

Table 2. Parameters of EI core magnetic circuit.

Symbol	Parameters	Unit
R_{s1}	Reluctance of E stator core 1	H^{-1}
R_{s2}	Reluctance of E stator core 2	H^{-1}
R_{sj}	Reluctance of E stator joint core	H^{-1}
R_{g1}	Reluctance of air gap	H^{-1}
R_{gj}	Reluctance of joint air gap	H^{-1}
R_{t1}	Reluctance of I translator core	H^{-1}
F	Magnetomotive force	At
ψ_1, ψ_y	Parallel magnetic fluxes	Wb
ψ	Total magnetic flux	Wb
ψ	Turn number of a coil	250

$$R_{g1} = \frac{2l_g}{\mu_0 l_{sy1}\left(w_{sp} + w_{tp}\right)} \tag{5}$$

$$R_{gj} = \frac{2l_g}{\mu_0 l_{sy2}\left(w_{sp} + w_{tp}\right)} \tag{6}$$

The total reluctance is calculated using the rules of parallel and serial circuits in Eq. (7). The phase inductance is given in Eq. (8).

$$\Sigma R = \frac{\left(R_{s1} + R_{s2} + R_{g1} + R_{t1}\right)^2}{2\left(R_{s1} + R_{s2} + R_{g1} + R_{t1}\right)} + R_{sj} + R_{gj} \tag{7}$$

$$L\left(x, i\right) = \frac{2N^2}{\Sigma R\left(x, i\right)} \tag{8}$$

Here, 2 is the number of the phase of coils. The magnetic flux (ϕ) and magnetic flux density (B) are calculated by Eq. (9) and Eq. (10). These fluxes and air gap flux density obtained from FEA solutions are shown in Figure 5.

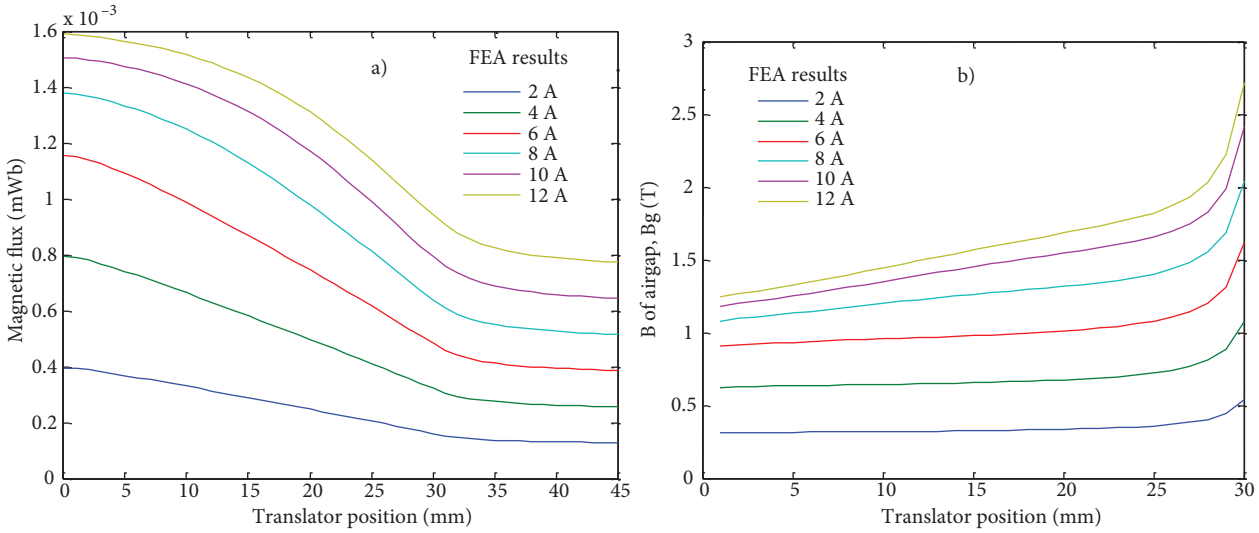

Figure 5. Magnetic field FEA solutions in air gap: a) flux (ψ), b) flux density (B).

$$\phi = \frac{F}{\Sigma R} = \frac{NI}{\Sigma R} \Longrightarrow \phi_1 = \phi_2 = \frac{\phi}{2} \tag{9}$$

$$B = \frac{\phi}{A} \tag{10}$$

B_g is presented between aligned and overlap positions. The cross-section of the air gap is smaller while the translator is moving and the core begins to saturate. The knee point of the BH curve is about 1.5 T. After the knee point the saturation starts in the core. Figure 6 presents magnetic flux densities in the EI core as magnitude and vector for three positions. In magnetostatic solutions, the excitation is 2000 At mmf (8A, 250 turns of a coil).

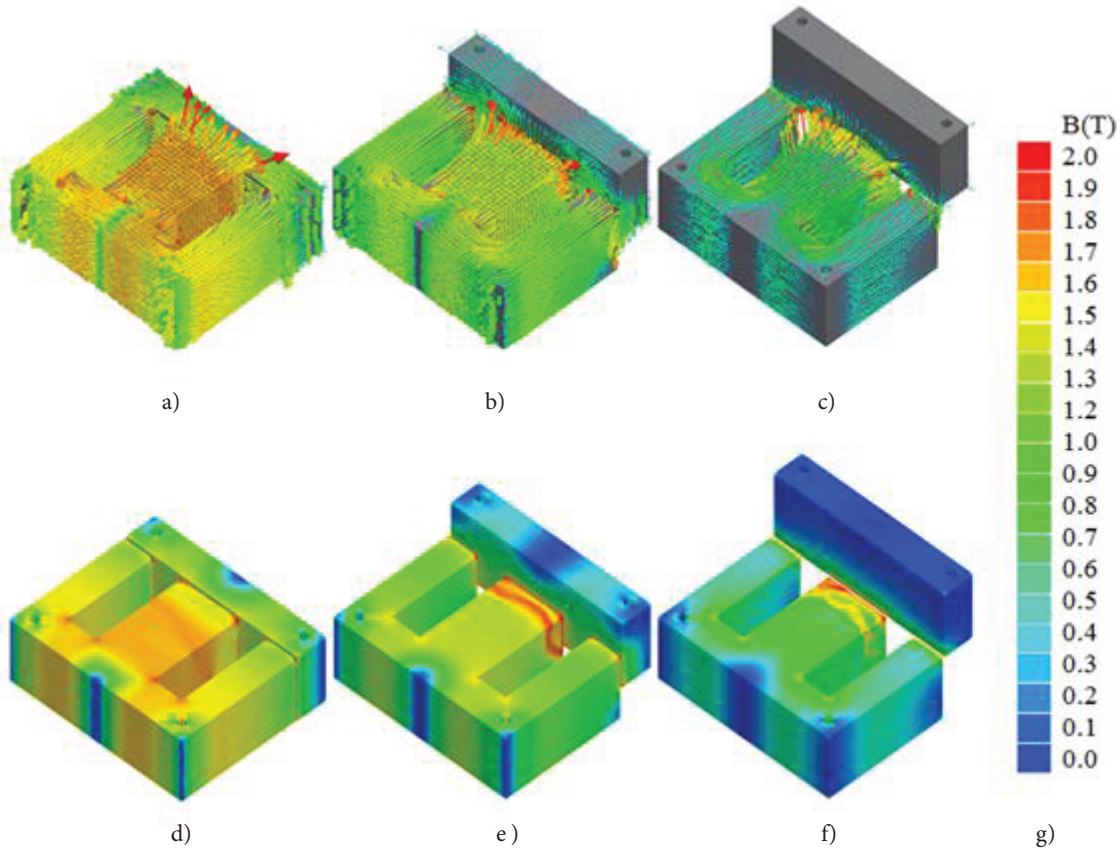

Figure 6. Distribution of magnetic flux density: a) vector B in aligned position (0), b) vector in midaligned position (15 mm), c) vector B in overlap position (30 mm), d) magnitude of B in aligned position (0), e) magnitude of B in midaligned position (15 mm), f) magnitude of B in overlap position (30 mm), g) B scale in tesla.

Figure 6 shows that the saturation effects, fringing and leakage flux, and nonuniform flux distributions are considered in FEA solutions. Only linear analytical predictions do not verify the electromagnetic model. Flux density at the corners of the core is lower because fluxes do not prefer rectangular paths. Circular core structures have advantages for uniform flux distribution [6]. In this design, packaging screw slots are placed at the corners of the core. The saturation effects of screw slots are very limited due to the weak fields at the corners.

4.2. Inductance

The phase inductance depends on the total reluctance, which varies according to translator position (x) and phase current (i). The inductance profile of the phase is affected because the BH curve of the core material is nonlinear [16]. Magnetic permeability is $\mu = \mu_r \mu_0$ and the ψ_r coefficient depends on the B/H ratio. Thus, as the phase current increases, the value of inductance is reduced. This situation is taken into consideration in the FEA. The phase inductance reaches its maximum value (L_a) at the aligned position (x = 0) and its minimum value (L_u) at unaligned positions (x = 45). Midway inductance (L_m) is obtained at the midway position (x = 22.5 mm). These positions are important to obtain the inductance profile in analytical calculations. If the values of the maximum, midway, and minimum inductances are calculated, phase inductance can be predicted by Eq. (12) for all positions. It is derived from the first three terms of the Fourier series via a curve fitting method [4,17]. Th phase inductance profile, which is experimentally verified, is shown in Figure 7. Phase inductance was measured with an LCR meter for each translator position.

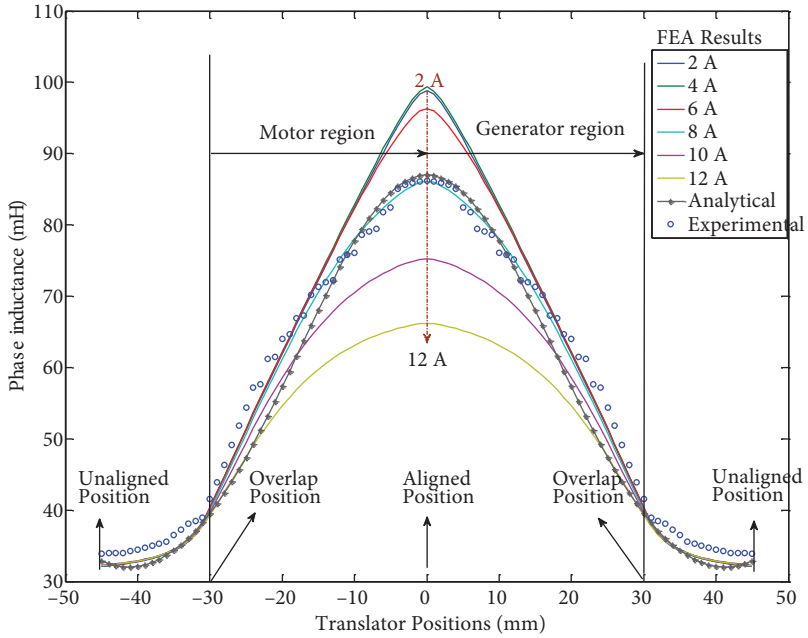

Figure 7. Phase inductance profile of EI core linear actuator.

$$L(x) = a_0 + a_1 \cos(k.n_{tp}x) + b_1 \cos(k.2n_{tp}x) \tag{11}$$

The Fourier coefficients a_0, a_1, and b_1 are given in Eq. (**??**) [17]. The k coefficient is necessary to convert the linear length into an angular value in the trigonometric expression and is given in Eq. (13) [6].

$$a_0 = \frac{1}{2}\left[\frac{L_a + L_u}{2} + L_m\right], a_1 = \frac{L_a - L_u}{2}, b_1 = \frac{1}{2}\left[\frac{L_a + L_u}{2} - L_m\right] \tag{12}$$

$$k = \frac{2\pi}{l_s} \tag{13}$$

Figure 7 shows the FEA solutions, analytical predictions, and experimental results. The phase inductance is reduced by current increases in FEA because of the saturation effects. Stator and translator have no back iron;

it is a yokeless design because the EI cores are separated from each other. Therefore, mutual inductance is so low that it can be neglected, but phase inductance includes the mutual inductance in analysis. Flux linkage in all translator positions is obtained from Eq. (14) [6] and is shown in Figure 8.

$$\lambda(x,i) = L(x,i)\, I \tag{14}$$

4.3. Forces

The actuator generates forces at 3 axes, which are propulsion (F_x), pull (F_z), and lateral (F_y) forces. Directions of the forces are given in Figure 9 [11]. Force components are calculated via Eq. (15) and Eq. (16) [11,18]. F_x provides the linear movement and the velocity of the actuator [8].

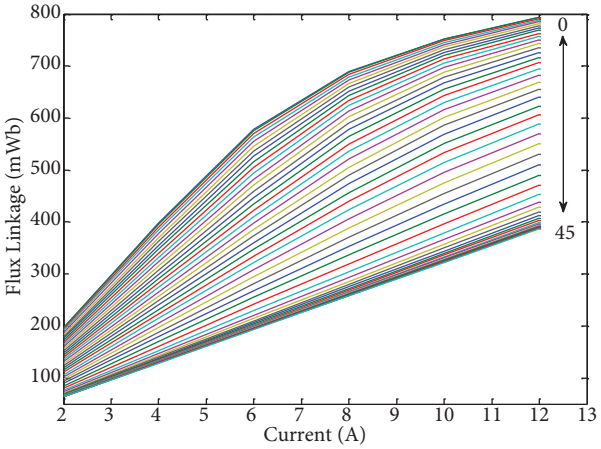

Figure 8. Flux linkage characteristic.

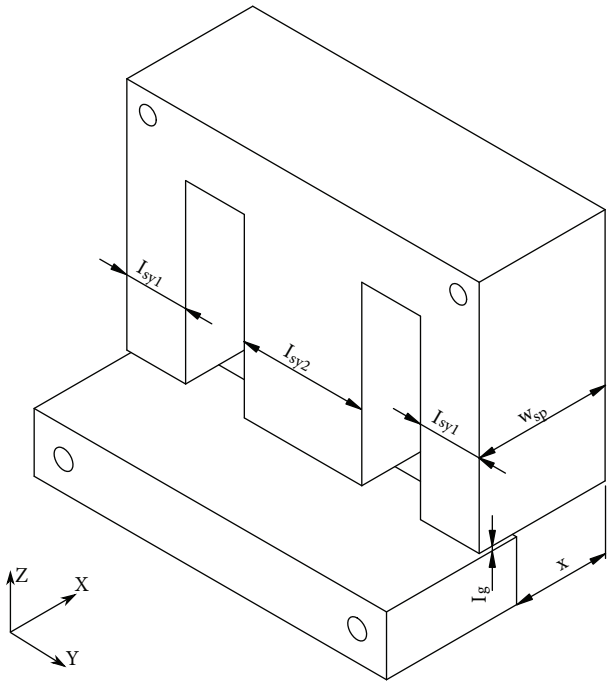

Figure 9. Force components of the actuator.

Lateral force F_y is zero because translator and stator are placed on the same movement axis. The magnitude of the pull force F_z is higher than propulsion force (F_x). These forces are shown in Figure 10. The translator can be deflected due to the pull force. For this reason, the air gap can be narrowed and kinetic friction can lead to mechanical problems. To avoid these problems, the pull force is mechanically restricted using a rail and bearing [7].

$$F_{x1} = \frac{B_g^2}{2\mu_0} YZ = \frac{B_g^2}{2\mu_0}(2l_{sy1} + l_{sy2})l_g \Longrightarrow F_x = 2F_{x1} \tag{15}$$

$$F_{z1} = \frac{B_g^2}{2\mu_0} XY = \frac{B_g^2}{2\mu_0}(2l_{sy1} + l_{sy2})(w_{sp} - x) \Longrightarrow F_z = 2F_{z1} \tag{16}$$

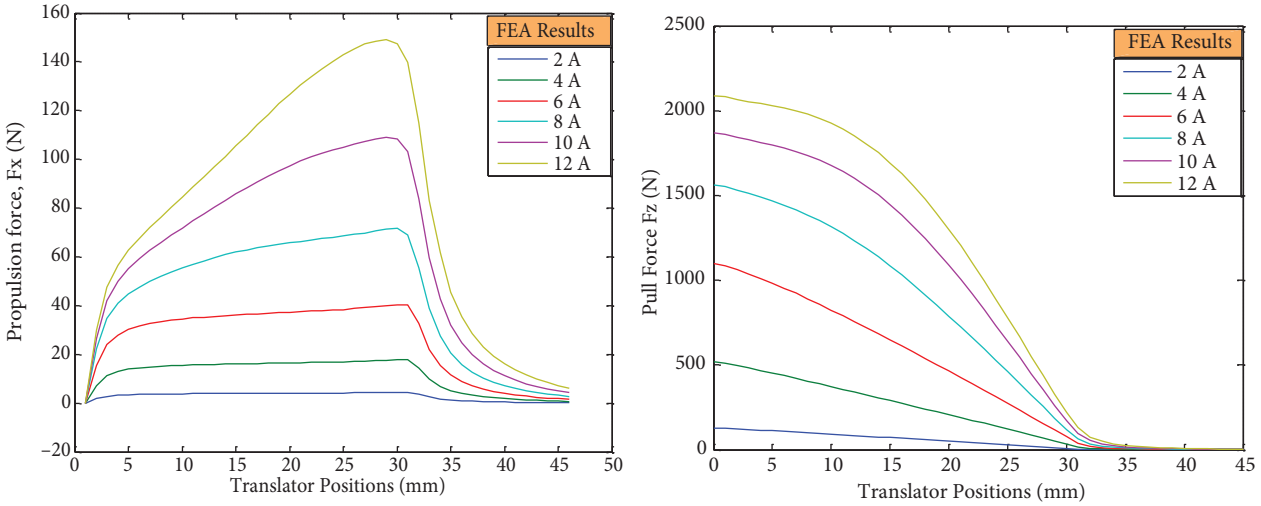

Figure 10. a) The propulsion force (F_x), b) the pull force (F_z).

4.4. Experiments

Force and phase inductance experimental setup is shown in Figure 11. The maximum propulsion forces are measured by a dynometer under the DC phase excitation conditions. Phase inductance is measured by an LCR meter. Their values are shown in Table 3. According to these results and saturation of the core, the optimal excitation current is 8A or 2000 At mmf because this is the knee point of the BH curve.

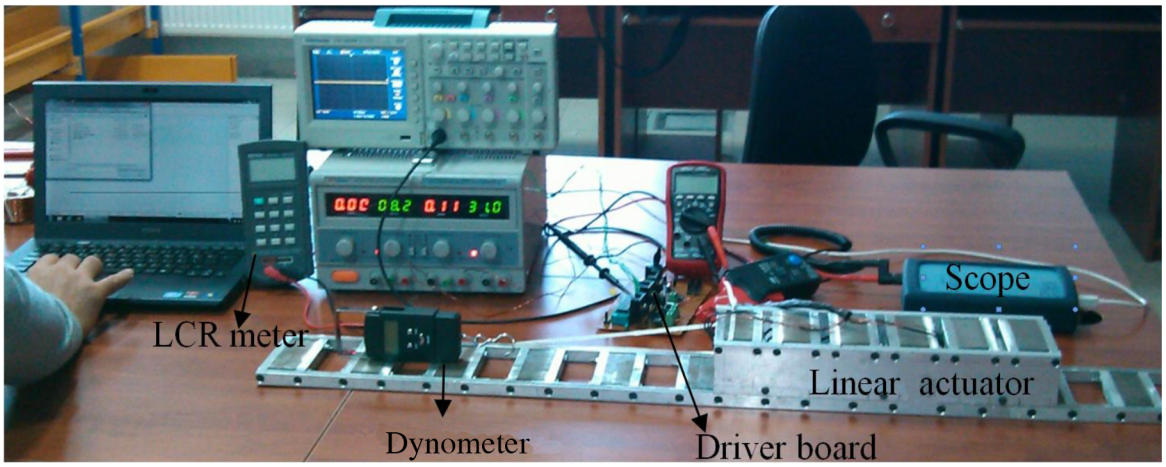

Figure 11. Force and phase inductance experimental setup.

Table 3. Experiments results.

Excitation current (A)	Voltage (V)	Propulsion force (N)	Power (W)
2	4.4	6.28	8.8
4	8.6	17.85	34.4
6	13.6	40.5	81.6
8	16.5	72.57	115.5

The maximum propulsion force and phase inductance are obtained by FEA via analytical approaches and experiments under 8 A DC phase excitation, which is rated current. Air gap flux density is assumed to be 1.3 T for analytical calculations. Table 4 shows that phase inductance and propulsion force solutions verify each other.

Table 4. Propulsion force solutions for 8 A excitation.

Excitation current (A)	Propulsion force (N)			Phase inductance (mH)					
	FEA	Analytical	Experiment	FEA		Analytical		Experiment	
				L_a	L_u	L_a	L_u	L_a	L_u
8	71.71	75.35	72.57	85.96	32.22	87.21	31.58	86.16	33.85

5. Conclusion

In this study, a linear actuator that has transverse flux and is single-sided is designed with an EI core structure. The stator and translator are combined with E and I shell cores. The actuator with three phases and 6/4 pole ratio is examined via FEA and is verified using analytical approximations. Magnetic fluxes at the core, air gap flux density, phase inductance, flux linkage, and axial forces are analyzed via 3D FEM. The BH characteristics, leakage flux, fringing, saturation, and mutual inductance are considered in FEA solutions. Propulsion force, power, and phase inductance are obtained by experiments. The measurements are verified by simulations and analytical predictions.

As the stator and translator parts are independent from each other, maintenance and repairing can be done easily by removing only the defective part. This provides a lower weight and lower cost. Moreover, the length of linear movement can be extended by adding new translator poles without changing the electromagnetic design. It implements electromechanical energy conversion as a direct drive. Linear movement is transferred magnetically so it does not require mechanical transmissions such as a pulley and chain drive. Thus, mechanical losses are low and periodical maintenance is not necessary. In the E core, magnetic flux density reaches 1.3 T, which is the knee point of the BH curve when the phase is excited with 2000 At mmf (8A, 250 turns). This is the optimal operation range because it is the starting point of the saturation. At this point, the actuator generates a maximum propulsion force of 72.57 N and the corresponding power consumption is 115.5 W. The air gap between the stator and translator is restricted with rail and bearings mechanically in order to eliminate the high pull force, which can cause mechanical problems. The actuator has a fault-tolerant design and it is proposed as an advantageous design for the horizontal transportation system, whereas the proposed actuator is suitable for linear automatic door systems, which can give rise to frequent failure.

References

[1] Amoros JG, Andrada P. Sensitivity analysis of geometrical parameters on a double-sided linear switched reluctance motor. IEEE T Ind Electron 2010; 57: 311–319.

[2] Iancu V, Popa DC, Szabo L. Fault tolerant linear transvere flux reluctance machines. J Comput Sci Contr Syst 2009; 2: 93–96.

[3] Baoming G, Almeida AT, Ferreira FJTE. Design of transverse flux linear switched reluctance motor. IEEE T Magn 2009; 45: 113–119.

[4] Daldaban F, Üstkoyuncu N. A new linear switched reluctance motor with maglev effect. In: International Conference on Electrical and Electronics Engineering; November 2008; Bursa, Turkey. pp. 420–422.

[5] Chang J, Kang DH, Kang A, Larisa S. Transverse flux reluctance linear motor's analytical model based on finite-element method analysis results. IEEE T Magn 2007; 43: 1201–1204.

[6] Fenercioğlu A. Design and magnetically analysis of circular flux linear actuator. Elektronika Ir Elektrotechnica 2010; 101: 21–26.

[7] Fenercioglu A, Dursun M. Design and magnetic analysis of a double sided linear switched reluctance motor. Przeglad Elektrotechniczny 2010; 86: 78–82.

[8] Dursun M, Fenercioglu A. Velocity control of linear switched reluctance motor for prototype elevator load. Przeglad Elektrotechniczny 2011; 87: 209–214.

[9] Lenin NC, Arumugam R. A novel linear switched reluctance motor: investigation and experimental verification. Songklanakarin Journal of Science and Technology 2011; 33: 69–78.

[10] Lim HS, Krishnan R. Ropeless elevator with linear switched reluctance motor drive actuation systems. IEEE T Ind Electron 2007; 54: 2209–2218.

[11] Krishnan R. Switched Reluctance Motor Drives. Washington, DC, USA: CRC Press; 2004.

[12] Gan WC, Cheung NCA. A low-cost linear switched reluctance motor with integrated position sensor for general-purpose three-phase motor controller. In: 27th Annual Conference of the IEEE Industrial Electronics Society; December 2001; Denver, CO, USA. pp. 468–473.

[13] Garcia Amoros J, Andrada Gacson P. Study of end effects on the performance of the linear switched reluctance motor. In: 11th Spanish-Portuguese Conference on Electrical Engineering; July 2009; Zaragoza, Spain. pp. 1–6.

[14] Torkaman H, Afjei A. Comprehensive study of 2-D and 3-D finite element analysis of a switched reluctance motor. Journal of Applied Sciences 2008; 8: 2758–2763.

[15] Kolomeitsev L, Kraynov D, Pakhomin S, Rednov F, Kallenbach, E, Kireev V, Schneider T, Böcker J. Linear switched reluctance motor as a high efficiency propulsion system for railway vehicles. In: SPEEDAM International Symposium on Power Electronics, Electrical Drives, Automation and Motion; June 2008; Ischia, Italy. pp. 155–160.

[16] Jang SM, Park JH, Choi JY, Cho HW. Analytical prediction and measurements for inductance profile of linear switched reluctance motor. IEEE T Magn 2006; 42: 3428–3430.

[17] Gao HF, Salmasi R, Ehsani M. Inductance model-based sensorless control of the switched reluctance motor drive at low speed. IEEE T Power Electr 2004; 19: 1568–1573.

[18] Gan WC, Cheung NC, Qiu L. Position control of linear switched reluctance motors for high-precision applications. IEEE T Ind Appl 2003; 39: 1350–1362.